Heat Transfer Modeling for Regeneratively Cooled Thrust Chambers

Hideyo Negishi, Hiroshi Otomo†, Akinaga Kumakawa**, Yu Daimon*, and Nobuhiro Yamanishi**

**Japan Aerospace Exploration Agency(JAXA), Tsukuba, Ibaraki, 305-8505, Japan*

†Advancesoft Corporation Minato-ku, Tokyo,107-0052, Japan

***Japan Aerospace Exploration Agency(JAXA), Kakuda, Miyagi, 981-1525, Japan*

Abstract

An in-house numerical heat transfer analysis tool, REGEN (REGENerative cooling analysis tool), for liquid rocket engine thrust chambers is developed for engineering design purpose in JAXA. This tool consists of quasi one-dimensional model for the coolant flow and three-dimensional heat conduction model to calculate thermal field inside thrust chambers using Nusselt-type correlation for hot gas side and coolant side heat transfer. This tool was validated by LOX/methane sub-scale hot firing test. The computed result showed good agreement with the measured data. However, the results strongly depended on the surface roughness in the cooling channels. As for the computational cost, it took only a few minutes for a single run about the LOX/methane cooled thrust chamber. As a result, it was confirmed that this tool has a potential to be a cost-effective design tool for predicting regenerative cooling performance. Some problems to be solved were identified so as to improve quantitative accuracy.

1. Introduction

Regenerative cooling is typically used in high pressure thrust chambers of liquid rocket engines in order to avoid thermal failures due to high heat load. The role of regenerative cooling in thrust chambers is to reduce wall temperature within a permissive level with minimal pressure loss in cooling channels. From the view point of engine cycle, heat pick-up in cooling channels is also essential to drive turbo-pumps especially for expander-type cycle engines like RL-10 series, VINCI, and LE-5B. Therefore, precise estimation of regenerative cooling performance has been a major issue in the design of regeneratively cooled thrust chambers.

The thermal phenomena in thrust chambers involve interactions among a number of process including: combustion and expansion of gas inside a thrust chamber, heat transfer from hot gas to a chamber wall via convection and radiation, heat conduction inside a chamber wall and convection to cooling channels. In order to estimate regenerative cooling performance like heat load on the hot gas side wall, wall temperature, pressure loss and temperature gain in cooling channels, the modeling of the combustion flow inside a combustion chamber, the coolant flow inside cooling channels, and heat conduction in structure is important. And these models should be coupled and solved simultaneously.

There are several methods from conventional 1D analysis based on Nusselt-type correlation to 3D CFD simulation [1-6]. Nowadays, 3D CFD simulation can be considered as the most effective approach to evaluate precisely regenerative cooling performance. The main advantage of 3D CFD is the universal character and the relative precision of the results compared to conventional analysis method. However, the simulation of the combustion flow or the coolant flow in thrust chambers by itself is still a challenging problem, because the computed results strongly depend on physical models like turbulence or combustion [7, 8]. And also, it usually takes a long time for a single run, and is not yet cost effective approach. On the other hand, for the purpose of optimization or engine system analysis, the fast and accurate estimation is indispensable. Therefore, the conventional analysis tool based on Nusselt-ype correlation is considered to be still useful so far for designers of liquid rocket engines.

In this study, a numerical heat transfer analysis tool, REGEN (**REGEN**erative cooling analysis tool) is developed for optimal design of cooling channels and as a regenerative cooling module for an engine cycle analysis tool. It consists of quasi one-dimensional model for the coolant flow and three-dimensional heat conduction model to calculate temperature field inside wall using Nusselt-type correlation for hot-gas side and coolant-side heat transfer.
In this paper, REGEN is validated by LOX/methane sub-scale hot firing test data, and computed results are compared to the measured data. The capability of this tool is also discussed.

2. Numerical Modeling

REGEN is a computer program for regenerative cooling performance analysis of liquid rocket engines. It is composed of three models for combustion flow, conduction in wall, and coolant flow in cooling channels. The detail of each model is described in the following sections.

2.1 Coolant Flow

The coolant flow inside cooling channels is modeled as quasi-1D flow. Regeneratively cooled thrust chambers have typically several hundred cooling channels in the circumferential direction. For the numerical procedure, only one half of a cooling channel is calculated on the assumption that all cooling channels have the same result. A cooling channel is divided into a number of computational cells along the longitudinal direction, as shown in Fig. 1. The governing equations are the following mass, momentum, and energy conservation law:

$$\frac{d}{dx}(\rho u A) = 0 \qquad \cdots (1)$$

$$\frac{d}{dx}\left(\rho u^2 A + pA\right) = p\frac{dA}{dx} - F_f \qquad \cdots (2)$$

$$\frac{d}{dx}\left[\rho u A\left(h + \frac{1}{2}u^2\right)\right] = Q_{LW} - Q_f \qquad \cdots (3)$$

where ρ, u, p, h are density, velocity, static pressure, and specific enthalpy respectively in a cooling channel. A is the cross sectional area of a cooling channel. x is the axial coordinate. F_f is viscous force due to wall shear stress. Q_{LW} is total heat transferred through the coolant side wall. Q_f is energy loss caused by viscous force. The thermodynamic and transport properties of coolants like hydrogen, methane, oxygen, and ethanol is evaluated using look-up tables based on the NIST REFPROP [9].

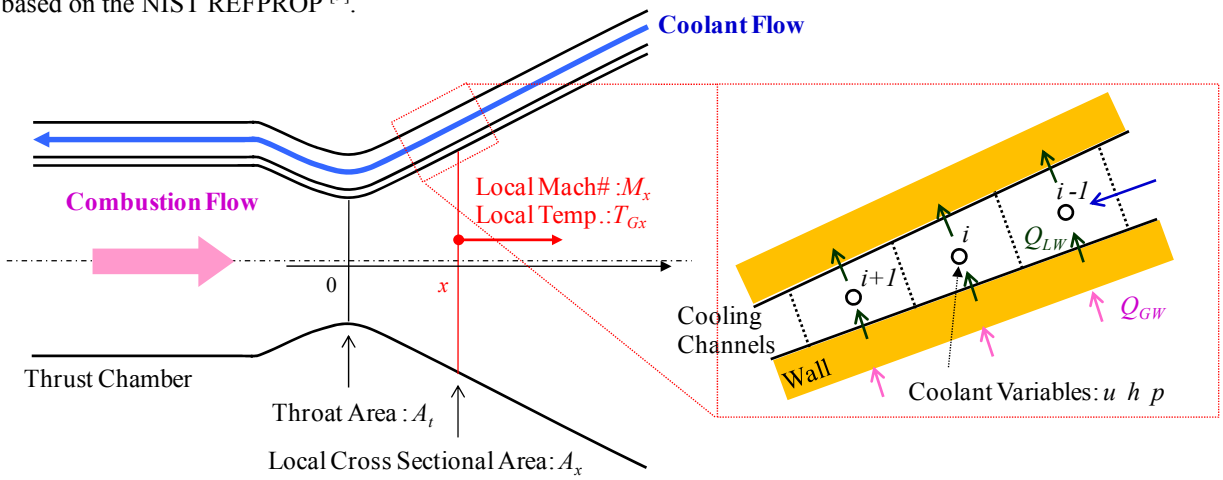

Figure 1: Numerical Model of a Regeneratively Cooled Thrust Chamber.

The Reynolds number Re based on the hydraulic diameter in the cooling channels is within the turbulent flow regime (up to 10^7). Therefore, the Darcy friction factor $f_{D,r}$ is calculated using the explicit formula [10] of the Colebrook equation given by:

$$\frac{1}{\sqrt{f_{D,r}}} = -2.0\log\left[\frac{\varepsilon}{3.7065 D_h} - \frac{5.0452}{\mathrm{Re}_b}\log\left(2.8257\left(\frac{\varepsilon}{D_h}\right)^{1.1098} + \frac{5.8506}{\mathrm{Re}_b^{0.8981}}\right)\right] \qquad \cdots (4)$$

where ε and D_h are the surface roughness and the hydraulic diameter of the cooling channels. The subscript b means the bulk property of the coolant flow. Eq. (4) is valid for non-heated tubes. However, cooling channels in thrust

chambers are heated asymmetrically by the combustion gas, which causes thermal stratification inside the channels. The thermal stratification strongly affects on the property variation and result in reduction of friction force in the cooling channels. Therefore, the following correction for the property variation proposed by Petkhov [11] is used:

$$f'_{D,r} = f_{D,r}\left(\frac{T_{LW}}{T_b}\right)^{-0.6+5.6\,\mathrm{Re}_w^{-0.38}} \quad \cdots (5)$$

where T_{LW} and T_b are the coolant side wall temperature and the bulk temperature of the coolant flow. $\mathrm{Re_w}$ is the Reynolds number based on the hydraulic diameter of the cooling channel and physical properties evaluated by T_{LW}.

Pressure drop due to sudden change of size in cooling channels like contraction or expansion is incorporated in Eq. (2) through the following equation [12]:

$$\Delta p = K\frac{1}{2}\rho u^2 \quad \cdots (6)$$

$$K = \begin{cases} \left(\zeta^{-2}-1\right)^2 & \text{for contraction} \\ 0.5-0.167\zeta-1.125\zeta^2-0.208\zeta^3 & \text{for expansion} \end{cases}$$

where ζ is the ratio of hydraulic diameter $D_{h,i}/D_{h,i-1}$. i denotes the computational node in a cooling channel, and i -1 means the upwind position.

The coolant side heat transfer in cooling channels of regeneratively cooled thrust chambers is generally evaluated by the following Nusselt-type formula:

$$Nu_{coolant,cal} = Nu_{coolant,s}\varphi_{ent}\varphi_{rough}\varphi_{curv} \quad \cdots (7)$$

where $Nu_{coolant,\,cal}$ is the local Nusselt number for calculation. $Nu_{coolant,\,s}$ is the local Nusselt number for a straight smooth tube at fully developed conditions. φ_{ent}, φ_{rough}, φ_{curv} are correction factors accounting for entrance, surface roughness and curvature effects in the cooling channels, respectively. The straight tube Nusselt number $Nu_{coolant,\,s}$ is evaluated by Taylor eq. [13] combined with the correction for property variation in cooling channels by Hendricks [14]:

$$Nu_{coolant,s} = 0.023\,\mathrm{Re}_b^{0.8}\,\mathrm{Pr}_b^{0.4}\,\Psi^{-0.55} \quad \cdots (8)$$

$$\Psi = 1+\beta\left(T_{LW}-T_b\right)$$

where Pr is the Prandtl number evaluated by bulk conditions. And β is the bulk expansion factor given by:

$$\beta = \frac{1}{\rho}\frac{\left(\partial p/\partial T\right)_\rho}{\left(\partial p/\partial T\right)_T} \quad \cdots (9)$$

The entrance factor φ_{ent} is calculated by the following equation for 90 deg. bend entrance [15]:

$$\varphi_{ent} = \left[1+\left(\frac{s}{D}\right)^{-0.7}\left(\frac{T_{LW}}{T_b}\right)^{0.1}\right] \quad \cdots (10)$$

where s is the distance from the starting point along a cooling channel.

The roughness factor φ_{rough} is determined by Nunner eq. [15] :

$$\varphi_{rough} = \frac{1+1.5\,\mathrm{Pr}_b^{-\frac{1}{6}}\,\mathrm{Re}_b^{-\frac{1}{8}}\left(\mathrm{Pr}_b-1\right)}{1+1.5\,\mathrm{Pr}_b^{-\frac{1}{6}}\,\mathrm{Re}_b^{-\frac{1}{8}}\left(\mathrm{Pr}_b\,\xi-1\right)}\xi \quad \cdots (11)$$

where ξ is the ratio of the rough tube friction factor to the smooth one and given by :

$$\xi = \frac{f_{D,r}}{f_{D,s}} \qquad \cdots (12)$$

The smooth tube friction factor $f_{D,s}$ is calculated by Nikuradse eq. :

$$f_{D,s} = 0.0032 + 0.221\,\mathrm{Re}_b^{-0.237} \qquad \cdots (13)$$

The curvature factor φ_{curv} is evaluated by Taylor eq [13]:

$$\varphi_{curv}(\pm) = \left[\mathrm{Re}_b \left(\frac{r_h}{R_c} \right)^2 \right]^{\pm 0.05} \qquad \cdots (14)$$

where r_h is the hydraulic radius, and R_c is the radius of curvature. The sign (+) denotes the concave curvature and the sign (-) denotes the convex one. This effect is considerd only at the curvature region.

2.2 Combustion Gas Flow

Assuming a quasi-1D isentropic flow, local Mach number and static temperature of the combustion gas flow is calculated along the hot gas side wall at each axial location, where hot gas side heat flux is evaluated. The thermodynamic and transport properties of the combustion gas are calculated by NASA CEA code (Chemical Equilibrium with Applications) [16, 17] incorporated into REGEN. The hot gas side heat transfer is given by the following formula:

$$h_{gas,cal} = h_{Bartz} \varphi_{inj} \varphi_{super} \qquad \cdots (15)$$

where h_{gas} is the local heat transfer coefficient on the hot gas side wall of thrust chambers. φ_{inj} and φ_{super} are the empirical correction factors for the injector end effect and supersonic expansion effect, respectively.

The local heat transfer coefficient is evaluated by Bartz eq. as follows:

$$h_{Bartz} = \frac{C_{Bartz}}{D_t^{0.2}} \left(\frac{\mu_0^{0.2} C_{p,0}}{\mathrm{Pr}_0^{0.6}} \right) \left(\frac{p_c}{c^*} \right)^{0.8} \left(\frac{D_t}{r_c} \right)^{0.1} \left(\frac{A_t}{A_x} \right)^{0.9} \sigma \qquad \cdots (16)$$

$$\sigma = \left\{ \frac{1}{2} \left[\frac{T_{GW}}{T_c} \left(1 + \frac{\gamma - 1}{2} M_x^2 \right) + 1 \right] \right\}^{\frac{\omega}{5} - 0.8} \left(1 + \frac{\gamma - 1}{2} M_x^2 \right)^{-\frac{\omega}{5}}$$

where C_{Bartz} is the heat transfer coefficent, which is generally set to 0.026 proposed in the original paper [18]. D is the diameter. μ and C_p are the viscosity and the specifitc heat at constant pressure, respectively. P_c and T_c is the combustion pressure and temperature. c^* is the characteristic velocity. r_c is the throat radius of curvature. A is the cross sectional area. T_{GW} is the hot gas side wall temperature. γ is the specific heat ratio. M is the Mach number. The subscripts *0*, *t*, *x* are the stagnation, the throat, and the local conditions, respectively. σ is the correction factor for property variation across the boundary layer. ω is typically set to 0.6.

The injector end effect φ_{inj} is an empirical function accounting for the increase of local hot gas side heat transfer due to the development of the boundary layer and the flame along the axial direction in the combustion gas. And this is modeled as follows [19]:

$$\varphi_{inj} = \min\left[\frac{2}{15} \bar{x}_c - \frac{1}{3}, 1.0 \right] \qquad \cdots (17)$$

$$\bar{x}_c = \frac{x_c + 0.4 U_r}{100 D_c / \sqrt{N}}$$

where x_c is the distance from the injector face plate, and $\bar{x}_c$ is the normalized one. U_r is the velocity ratio of the propellant injections. D_c is the diameter of the cylinder part of thrust chambers. N is the number of injector elements.

The correction factor φ_{super} is an empirical function of local Mach number for supersonic expansion region. The original Bartz eq. generally overestimates heat flux in the region downstream the throat [19]. The effect of this correction factor is to lower heat flux there. On the other hand, in some cases, Mayer eq. [21] can produce better solution compared to equation 15 for a supersonic expansion region. Mayer eq. is derived from a approximate solution of energy-integral equations for the bounday layer and given by the following formula:

$$h_{gas,cal} = h_{Mayer} = \frac{B\eta^{\frac{1}{1-b}} r^{\frac{b}{1-b}} \left(\rho_\infty U_\infty\right)_x C_{p,0} \,\mathrm{Pr}_0^{-\frac{2}{3}}}{\left[\int_0^s (r\eta)^{\frac{1}{1-b}} \left(\frac{\rho_\infty U_\infty}{\mu_\infty}\right)_x ds\right]^b} \qquad \cdots (18)$$

$$\eta = \left(\frac{T_{\infty,x}}{T^*}\right)^{1-b(1+\theta)}$$

$$\theta = \frac{\ln\left(\mu_e/\mu_0\right)}{\ln\left(T_e/T_0\right)}$$

$$T^* = 0.5\left(T_{GW,x} + T_{\infty,x}\right) + 0.22\left(T_{ad} - T_{\infty,s}\right)$$

where B and b are the semi-empirical Blasius parameters, those values are listed in Table 1. U is the velocity. T_{ad} is the adiabatic wall temperature. θ is the viscosity-temperature exponent. T^* is the reference temperature. The sub-scripts ∞, 0, e, and x are the free stream, the stagnation, the exit, and the local conditions, respectively. s is the longitudinal coordinate with origin s = 0 at the injector, and r is the radius of rotation at the coordinate s.

Table 1: Semi-empirical Blasius Parameters

Flow in boundary layer	b	B
Laminar	1/2	0.332
Turbulent	1/5	0.0296

2.3 Heat Conduction in Wall

The wall structure is thermally coupled to the thermal field of the cooling channel flow. The 3D heat conduction equation is solved by the finite volume method using the structured grid system, as shown in Fig. 2. The governing equation is given by:

$$\frac{d}{dt}\int_{CV} \rho_W C_W T_W dV = \int_S \vec{q}\cdot d\vec{S} \qquad \cdots (19)$$

where ρ_W, C_W, and T_W are the density, the specific heat, and the temperature of wall. V is the volume of a control volume. S is the surface area of a cell interface. For numerical procedure, the left hand side in eq. (20) can be set to zero since a steady state solution is only taken into account. The systems of algebraic equations of temperature are solved by an iterative method, Bi-CGSTAB [21].

2.4 Overall Numerical Procedure

The Flowchart of the overall numerical procedure in REGEN is shown in Fig. 3. After initial setting, the program marches along the coolant flow direction. At each node, the hot gas side and the coolant side heat transfer coefficients are calculated. Then, velocity, static pressure, and specific enthalpy are renewed solving equations (1), (2) and (3) from one node to another. 3D wall temperature distribution is calculated solving eq. (19) with Bi-CGSTAB. The procedure described above is to be repeated iteratively until the solution is converged.

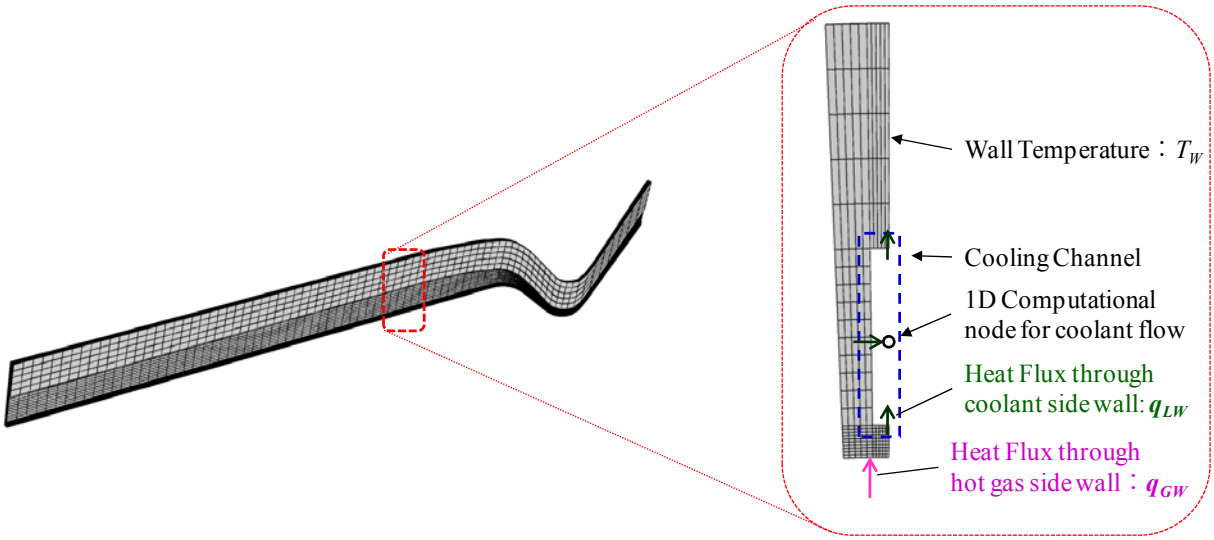

Figure 2: 3D Heat Conduction Model.

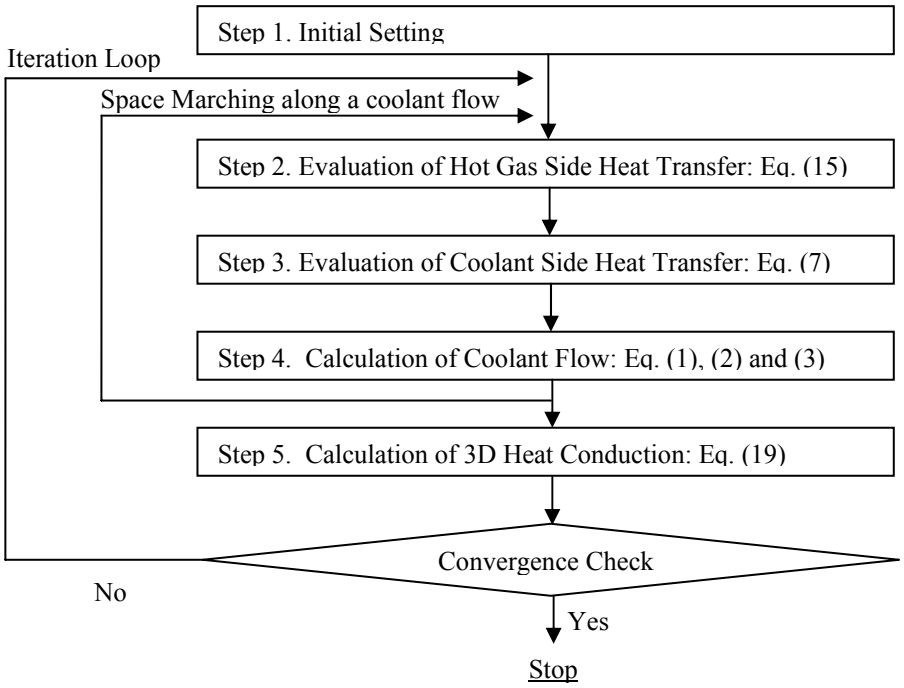

Figure 3: Flowchart of Overall Numerical Procedure.

3. Results and Discussion

In this section, the application of the newly developed tool described above, REGEN, to sub-scale thrust chambers is presented. In order to validate the capability of REGEN, numerical simulations for LOX/methane sub-scale thrust chambers with multi-injector elements were performed. Two cases were selected. Firstly, the simulation for a LOX/methane sub-scale water-cooled calorimeter chamber was carried out to validate the hot gas side heat transfer prediction. Secondary, one for a liquid methane cooled thrust chamber was conducted to validate the coolant side heat transfer and the coolant flow prediction. These simulations and hot firing tests were conducted under the conceptual design study of a LOX/methane regeneratively cooled engine in JAXA. [22] In the simulations, the carbon deposition on the hot gas side wall and the coke formation on the coolant side wall are not taken into account for simplicity.

3.1 Validation of Hot Gas Side Heat Transfer

The hot firing test for the LOX/methane sub-scale water-cooled calorimeter chamber was carried out to investigate the hot gas side heat transfer characteristics at JAXA/Kakuda Space Center in 2007. The typical specifications are presented in Table 2.

The hot gas side heat flux was calculated by the original Bartz eq.(eq. 16) and the modified one (eq. 15) using two values of C_{Bartz}, 0.026 and 0.023. The result calculated by Mayer eq. (eq. 18) is also plotted. The example of computed results were shown in Fig. 4, and compared to the experimental results. Near the face plate, the modified Bartz eq. (eq. 15) shows good agreement compared to the original Bartz eq. This indicates that the correction factor φ_{inj} predicts well the development of the boundary layer along the wall and the flame inside the thrust chamber. The Mayer eq. overpredicts wall heat flux there, producing considerably high value at the face plate. This is because the denominator of eq. 18 is nearly zero due to integration by s. In the region downstream of the throat, the original Bartz eq. overpredicts wall heat flux, and the modified Bartz. eq. underpredicts it a little. On the other hand, the result of Mayer eq. is in a better agreement. Regarding the value of C_{Bartz}, 0.026 predicts well heat flux peak, but overpredicts heat flux on the cylinder section, from x = -0.23 to -0.1. On the contrary, 0.023 shows a good agreement on the cylinder section, although the heat flux peak at the throat is underestimated. The result described above indicates that the hybrid method using the modified Bartz eq. and the Mayer eq. can predict hot gas side heat flux well. In the following section, the modified Bartz. eq, in which C_{Bartz} is set to 0.023, is used from the face plate to the region near the throat. In the supersonic region, the Mayer eq. is used. The switching between two equations is simply done as follows:

$$h_{gas,cal} = \max\left[h_{Bartz}\varphi_{inj}\varphi_{super},\quad h_{Mayer}\right] \quad \text{if } x > 0.0 \text{ (Supersonic region)} \qquad \cdots (20)$$

Table 2: Specifications of Water-cooled Calorimeter Chamber.

Chamber Pressure	5.85 MPa
O/F(mixture ratio)	3.3
c^* efficiency	0.92
Throat diameter	28 mm
Number of injector elements	20

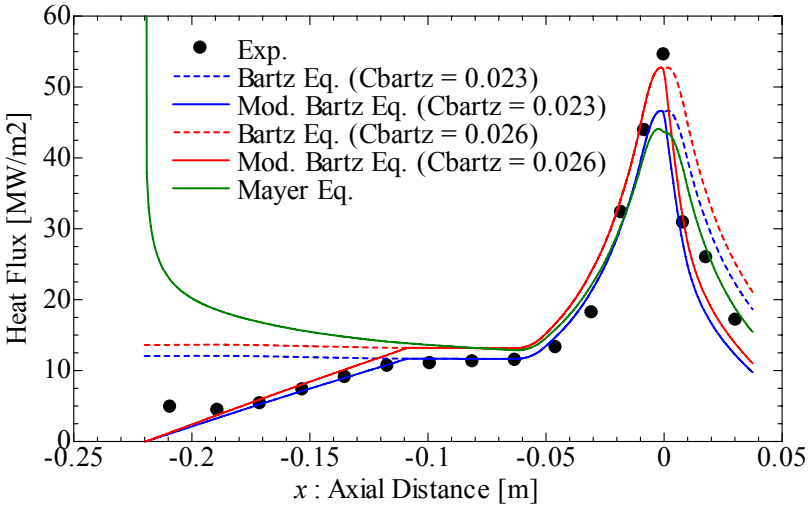

Figure 4: Hot Gas Side Wall Heat Flux.

3.1 Validation of Coolant Side Heat Transfer and Coolant Flow

The hot firing test for the sub-scale liquid cooled thrust chamber was also conducted to investigate the coolant side heat transfer characteristics at JAXA/Kakuda Space Center in 2007. The thrust chamber consists of a copper inner liner with 66 milled cooling channels, a copper electroforming layer and a stainless steel outer shell. The injector head is composed of 20 injector elements. The typical specifications are presented in Table 3.

Table 3: Specifications of Liquid Methane Cooled Thrust Chamber.

Chamber Pressure	5.96 MPa
O/F(mixture ratio)	3.6
c^* efficiency	0.90
Throat diameter	28 mm
Number of injector elements	20
Number of Cooling Channels	66
Coolant	Liquid methane
Coolant inlet pressure	8.28 MPa
Coolant inlet temperature	119 K
Coolant mass flow rate	1.05 kg/sec

The total and the static pressure distributions in the cooling channels are plotted in Fig. 5. The position of the throat corresponds to $x = 0$ in the horizontal axis. In order to investigate the influence of surface roughness in the cooling channels, 4 and 35 micron are used for simulations. The results indicate that the pressure profile strongly depends on the surface roughness. 4 micron is selected to match pressure loss inside the cooling channels with the measured data. 35 micron is an averaged value measured after hot firing tests. The total pressure decreases monotonically along the cooling channel. On the other hand, static pressure decreases steeply near the throat, which is caused by the increase of coolant velocity due to reduced size of the cooling channels there.

Figure 6 shows the coolant static temperature distributions. The results indicate again that the surface roughness in the cooling channels strongly influences on the temperature profile, especially from the upstream of the throat to the nozzle exit. The slope of the profile for the 35 micron case in this region is smaller than that for the 4 micron case. This is due to the specific heat at constant pressure steeply increased in the cooling channels, which is shown in Fig. 7. Near the throat, the static pressure and temperature for the 35 micron case are closer to the critical point of methane, 4.60 MPa and 190.56 K, which results in larger specific heat at constant pressure due to the near-critical behaviour of methane compared to the 4 micron case. Such large specific heat at constant pressure for the 35 micron case reduces the gain of static temperature in this region.

Figure 8 displays the wall temperature contour plot for the 4 micron case. For purpose of visualization, the computed result of one cooling channel is copied in the circumferential direction. The maximum wall temperature can be seen on the hot gas side wall near the throat. The wall temperature globally increases along the combustion gas flow. Wall temperature contour plots in the cross section at the throat are shown in Fig. 9. The large temperature gradient in the radial direction can be seen between the hot gas side wall and the coolant side lower wall. The results of the 4 micron and the 35 micron cases are almost the same in this axial position. Figure 10 is the wall temperature distributions on the hot gas side wall, the coolant side lower wall, and the coolant side upper wall in the axial direction. The measured temperature in the copper inner liner and the copper electroforming layer is also plotted in this figure. The maximum wall temperature is observed on the hot gas side wall at the throat. Wall temperature profiles depend on the surface roughness. The wall temperature for the 35 micron case is globally lower than that for the 4 micron case. This is because the surface roughness enhances the heat transfer on the coolant side wall and reduces wall temperature. The computed wall temperature agrees well with the measured one in the copper inner lin-

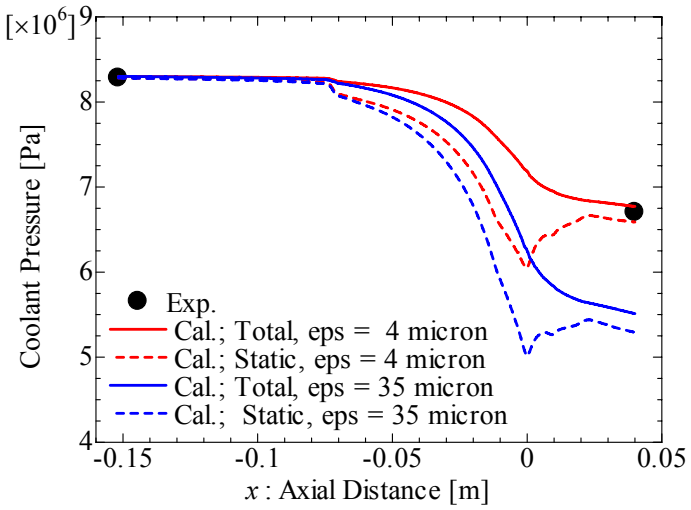

Figure 5: Coolant Pressure in the Cooling Channels.

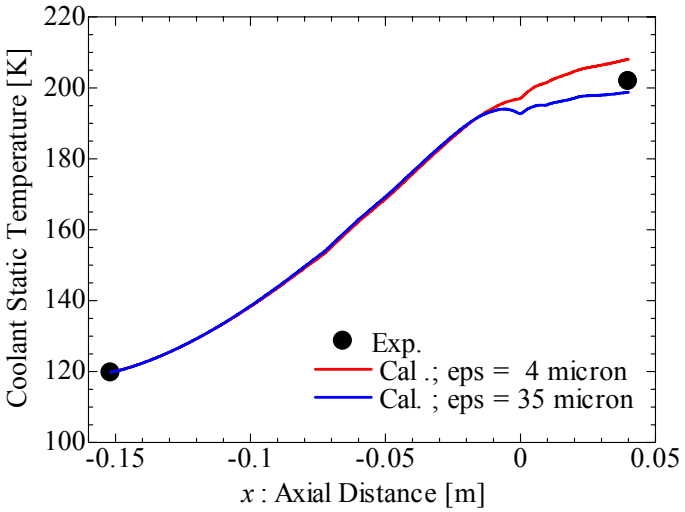

Figure 6: Coolant Temperature in the Cooling Channels.

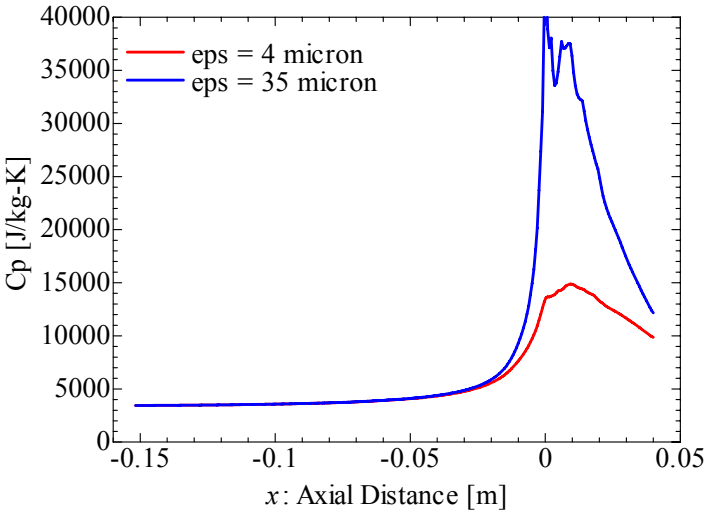

Figure 7: Specific Heat at Constant Pressure in the Cooling Channels.

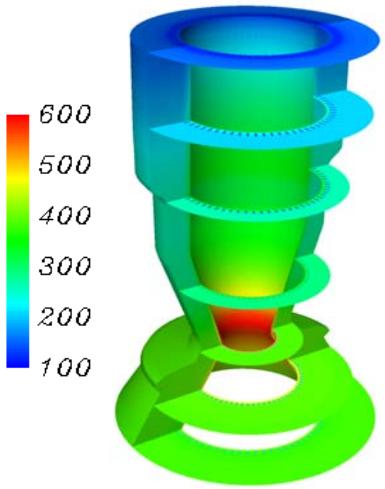

Figure 8: 3D View of Wall Temperature Distribution.; Surface roughness is 4 micron, Unit is [K]

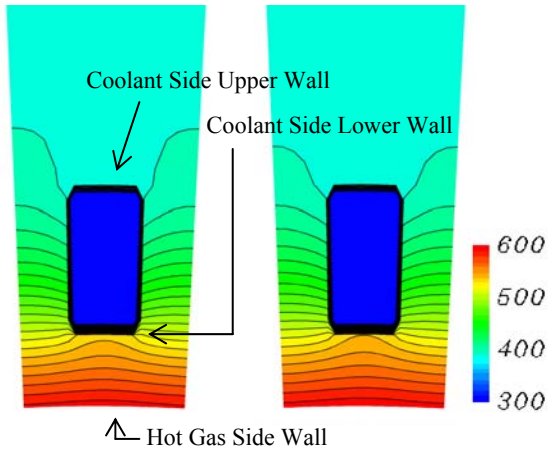

(a) 4 micron case **(b) 35 micron case**

Figure 9: Wall Temperature Contour Plots on the Cross Section at the Throat.; Unit is [K]

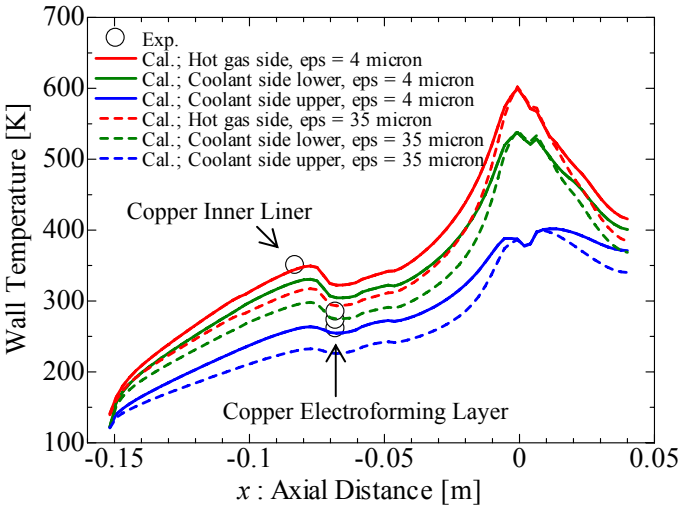

Figure 10: Wall Temperature Distributions in the Axial Direction.

er and the electroforming layer. However, it should be noted that the current numerical model is based on the homogenous flow assumption in the cross section and can underestimate wall temperature, because the thermal stratification effect is not taken into account. In reality, inhomogeneous temperature distribution in the cross section occurs and acts like a thermal barrier between the coolant side wall and the coolant core flow, which degrades the heat transfer and causes higher wall temperature.[4]

Regarding the computational cost, it takes about 5 minute for a single run for this sub-scale liquid methane cooled thrust chamber, using 1 CPU of Xeon 3.0 GHz. From the viewpoint of the engineering design, it is clear that REGEN has a potential to be a cost effective tool for regenerative cooling performance analysis.

4. Summary and Future Works

A numerical heat transfer analysis tool, REGEN, is developed for engineering design purpose. It consists of quasi one-dimensional model for the coolant flow and three-dimensional heat conduction model to calculate temperature field inside wall using Nusselt-type correlation for hot-gas side and coolant-side heat transfer. In order to validate the capability of this developed tool, numerical simulations were performed for LOX/methane sub-scale thrust chmabers. As for the hot gas side heat transfer prediction, computed heat flux distribution agree well with the result of the water-cooled calorimeter thrust chamber. Combined method with the modified Bartz. eq. and Mayer eq. shows better agreement. Regarding the coolant side heat transfer and the coolant flow prediction, the computed

coolant pressure and temperature as well as wall temperature agree well with the experimental results of methane cooled thrust chamber. However, the results strongly depend on the surface roughness in the cooling channels. For now, surface roughness tuning is required to match the pressure drop in the cooling channels with the measured data. This tool only takes about several minutes for a single run to be complted. As a result, it was confirmed that this tool has a potential to be a cost-effective analysis tool for predicting regenerative cooling performance.

Further improvements are expected for quantitative accuracy. The surface roughness effect on coolant friction force should be upgraded in order to remove parameter tuning about pressure drop in the cooling channels. Thermal barrier effect due to thermal stratification in the cross section on coolant side heat transfer is expected to be introduced for more precise thermal field prediction. In addition, non-uniformity of hot gas side heat flux in the circumferential direction, pressure drop between a manifold and cooling channels, and radiation heat transfer to wall from the combustion gas should be taken into account for better precision.

References

[1] Omori, S., et al, "Wall Temperature Distribution Calculation for A Rocket Nozzle Contour," NASA TN D-6825, July, 1972.

[2] Fröhlich, A., et al., "Heat Transfer Characteristics of H2/O2 –Combustion Chambers," AIAA Paper 93-1826, June, 1993.

[3] Wang, T.-S., et al., "Hot-Gas-Side and Coolant-Side Heat Transfer in Liquid Rocket Engine Combustors," *Journal of Thermophysics and Heat Transfer*, Vol. 8, No. 3, July-Sept., 1994, pp. 524-530.

[4] Woschnak, A., et al., "Thermo-and Fluidmechanical Analysis of High Aspect Ratio Cooling Channels," AIAA Paper 2001-3404, July, 2001.

[5] Naraghi, M.H., et al., "A Model for Design and Analysis of Regeneratively Cooled Rocket Engines," AIAA Paper 2004-3852, July, 2004.

[6] Knab, O., et al., "Advanced Combustion and Heat Transfer Modeling in Rocket Thrust Chamber Applied Engineering," 2007 International Symposium on Space Propulsion, Beijing, China, Oct. 8-12, 2007.

[7] Mews, B., et al., "Cooling Side Heat Transfer Analysis for High Performance Rocket Combustion Chambers," 4th International Conference on Launcher Technology 'Space Launcher Liquid Propulsion', Liege, Belgium, Dec. 3-6, 2002.

[8] Tucker, P. K., et al., "Validation of High-Fidelity CFD Simulations for Rocket Injector Design," AIAA Paper 2008-5226, July 21-23, 2008.

[9] NIST Reference Fluid Thermodynamic and Transport Properties Database (REPFROP):Ver. 8.0, The National Institute of Standards and Technology, 2007; http://www.nist.gov/srd/nist23.htm.

[10] Cheng, N. H., "An Explicit Equation for Friction Factor in Pipe," *Ind. Eng. Chem. Fundam*, Vol. 18, No. 3, 1979, pp. 296-297.

[11] Petkhov, B. S., *Prog. Heat & Mass Transfer*, Vol. 6, 1970.

[12] Naraghi, M. H. N., "RTE – A Computer Code for Three-Dimensional Rocket Thermal Evaluation," User Manual, 2002; http://home.manhattan.edu/~mohammad.naraghi//rte/rte.html.

[13] Taylor, M. F., "Method of Predicting Heat Transfer Coefficients the Cooling Passages of NERVA and PHOEBUS-2 Rocket Nozzles," NASA TM X-52437, 1968.

[14] Hendricks, R. C., et al., "Heat Transfer Characteristics of Cryogenic Hydrogen from 1000 to 2500 psia Flowing Upward in Uniformly Heated Straight Tubes," NASA TN D-2977, 1965.

[15] Niino, M. et al., "Heat Transfer Characteristics of Liquid Hydrogen as a Coolant for the LO2/LH2 Rocket Thrust Chamber with the Channel Wall Construction," AIAA Paper 82-1107, June, 1982.

[16] Gordon, S., and McBride B. J., "Computer Program for Calculation of Complex Chemical Equilibrium Compositions and Applications; I. Analysis, " NASA RP-1311, Otc., 1994.

[17] McBride, B., J., and Gordoin, S., "Computer Program for Calculation of Complex Chemical Equilibrium Compositions and Applications; II. Users Manual and Program Description," NASA RP-1311, Oct., 1996.

[18] Bartz, D., R., "A Simple Equation for Rapid Estimation of Rocket Nozzle Convective Heat Transfer Coefficient," *Jet Propulsion*, Vol. 27, No. 1, Jan., 1957, pp. 49-51.

[19] Kumakawa, A., et al., "Hot Gas Side Heat Transfer Characteristics of LOX/H2 and LOX/HC Type Propellants," Technical Report of National Aerospace Laboratory, TR-1062T, April, 1990.

[20] Mayer, E., "Analysis of Convective Heat Transfer in Rocket Nozzles," *ARS Journal*, Vol. 31, No. 7, Jan., 1961, pp. 911-916.

[21] Van der Vorst, H. A., "Bi-CGSTAB: A Fast and Smoothly Converging Variant of Bi-CG for the Solution of Nonsymmetric Linear Systems," *SIAM J. Sci. Stat. Comput.*, Vol. 13, 1992, pp. 631-644.

[22] Kawashima, H., et al., "Combustion and Regenerative Cooling Characteristics of LOX/Methane Engine," AIAA Paper 2008-4837, July, 2008.